Geophysical Prospecting

EAGE EUROPEAN ASSOCIATION OF GEOSCIENTISTS & ENGINEERS

Geophysical Prospecting, 2019, **67**, 2402–2413 doi: 10.1111/1365-2478.12869

P-wave complex-valued traveltimes in homogeneous attenuating transversely isotropic media

Qi Hao[1]*, Umair bin Waheed[1] and Tariq Alkhalifah[2]

[1]*College of Petroleum Engineering and Geosciences, King Fahd University of Petroleum and Minerals, Dhahran 31261, Saudi Arabia, and* [2]*Physical Science and Engineering Division, King Abdullah University of Science and Technology, Thuwal 23955, Saudi Arabia*

Received February 2019, revision accepted August 2019

ABSTRACT

Computation of complex-valued traveltimes provides an efficient approach to describe the seismic wave attenuation for applications like attenuation tomography, inverse Q filtering and Kirchhoff migration with absorption compensation. Attenuating acoustic transverse isotropy can be used to describe the directional variation of velocity and attenuation of P-waves in thin-bedding geological structures. We present an approximate method to solve the acoustic eikonal equation for an attenuating transversely isotropic medium with a vertical symmetry axis. We take into account two similar parameterizations of an attenuating vertical symmetry axis medium. The first parameterization uses the normal moveout velocity, whereas the second parameterization uses the horizontal velocity. For each parameterization, we combine perturbation theory and the Shanks transform in different ways to derive analytic solutions. Numerical examples show that the analytic solutions derived from the second parameterization yield better accuracy. The Shanks transform solution with respect to only the anellipticity parameter from the second parameterization is demonstrated numerically to be the most accurate among all the analytic solutions.

Key words: Anisotropy, Attenuation, Travel time.

INTRODUCTION

Seismic wave propagation in the Earth exhibits attenuation. In an attenuating medium, ray traveltimes of time-harmonic body waves are generally complex valued and are governed by the complex-valued eikonal equation (Červený and Pšenčík 2009). The real part of the complex-valued traveltimes corresponds to the phase of the seismic wave, while the imaginary part admits a decay in the amplitude due to energy absorption. Computation of complex-valued traveltimes is useful for many applications including attenuation tomography, inverse Q filtering and Kirchhoff migration with absorption compensation. Horizontal fine layering is a common geological phenomenon in the subsurface that causes effective attenuating transverse isotropy with a vertical symmetry axis (VTI). As a classic example of fine layering, shale is observed experimentally to be of attenuating transverse isotropy (e.g. Zhubayev *et al.* 2015).

For an attenuating VTI medium, the velocity and attenuation have the same symmetry. The combination of Thomsen's (1986) and Zhu and Tsvankin's (2006) notations can be used to describe the variation of velocity and attenuation with wave propagation direction in an attenuating VTI medium. In these notations, the shear-wave velocity parameter v_{S0} and the attenuation coefficient parameter A_{S0} are also included to characterize the exact P-wave velocity and attenuation. However, the influence of these parameters on the P-wave velocity and attenuation is extremely weak (Tsvankin and Thomsen 1994; Alkhalifah 1998; Zhu and Tsvankin 2006; Hao and Alkhalifah 2017b). Hence, ignoring the parameters v_{S0} and A_{S0} barely affects the complex-valued traveltimes in an attenuating anisotropic medium. Using this approximation, Hao and Alkhalifah (2017a, b) derived the acoustic attenuating eikonal equations for VTI and orthorhombic media.

*E-mail: xqi.hao@gmail.com

The attenuating eikonal equation is classified mathematically as a non-linear partial differential equation with complex coefficients. For inhomogeneous attenuating media, numerical techniques are needed to solve the attenuating eikonal equation. They include the complex ray method (e.g. Kravtsov, Forbes and Asatryan 1999), the real ray method (e.g. Vavryčuk 2008, 2012) and the real ray method based on perturbation theory (e.g. Červený and Pšenčík 2009). All these methods are ray based, that is, they calculate traveltimes using the ray tracing equations rather than directly solve the attenuating eikonal equation. Numerical techniques to directly solve the attenuating eikonal equation have received little attention so far. A review of the existing methods to solve the attenuating eikonal equations can be found in Hao and Alkhalifah (2017b).

For a homogeneous medium, the exact solution of the attenuating eikonal equation can be computed using a ray-based approach. The exact eikonal solution is given by the ray propagation distance divided by the complex ray velocity. The ray direction is always real valued in homogeneous attenuating media. The complex ray velocity can be indirectly obtained by numerically solving a system of non-linear equations (Vavryčuk 2006, 2007).

Compared with the ray-based approaches, the analytic solution of the attenuating eikonal equation is straightforward and convenient to implement. Hao and Alkhalifah (2017a, b) proposed a method combining a perturbation method and the Shanks transform to obtain analytic solutions to the acoustic attenuating VTI and orthorhombic eikonal equations. They choose the anellipticity and attenuation-anisotropy parameters as the perturbation parameters. In their method, the reference medium is attenuating and the coefficients of the traveltime expansion are always complex valued. Because of the complex eikonal equation in the reference medium, however, it is difficult to implement their perturbation method in the case of inhomogeneous media.

In this paper, we revisit the acoustic attenuating VTI eikonal equation to find the analytic solutions in the case of homogeneous media. We utilize two parameterizations and combine the perturbation theory and the Shanks transform to derive the analytic traveltime solutions. For each parameterization, we take into account an acoustic non-attenuating elliptically isotropic medium as the background. In this case, not only the reference eikonal equation but also the governing equations for the traveltime coefficients are real valued. Hence, it is easy to implement the method in the case of inhomogeneous media. We compare the accuracy of these solutions to investigate the effect of parameterizations on the traveltime approximation. Compared with the approaches discussed in Hao and Alkhalifah (2017a, b), we show that our new method needs less perturbation parameters and the coefficients of our traveltime expansion are real valued, which is more convenient for numerical implementations.

THEORY

In this section, we develop an approximate method for solving the acoustic eikonal equation (Hao and Alkhalifah 2017a) for a homogeneous attenuating vertical symmetry axis (VTI) medium. We consider two parameterizations of the acoustic attenuating VTI medium. The following five parameters are common to both parameterizations:

1. v_z – the P-wave vertical velocity;
2. η – the anellipticity anisotropy parameter (Alkhalifah 2000);
3. A_z – the P-wave vertical wavenumber-normalized attenuation coefficient (or briefly the attenuation coefficient), where the wavenumber is defined as the number of radians per unit distance, also referred to as the angular wavenumber;
4. ϵ_Q – the attenuation-anisotropy parameter describing the fractional difference between the horizontal and the vertical attenuation coefficients;
5. δ_Q – the attenuation-anisotropy parameter that controls the curvature of the attenuation coefficient curve in the vertical direction.

The two parameterizations differ in using the normal moveout (NMO) velocity v_n (Parameterization 1) and the horizontal velocity v_x (Parameterization 2).

For both parameterizations, the velocity-related parameters v_z, v_n, v_x and η are defined in the non-attenuating reference VTI medium corresponding to the real part of the complex stiffness coefficients. However, the attenuation-related parameters A_z, ϵ_Q, δ_Q are defined in the attenuating VTI medium. A detailed description of the attenuation-related parameters can be found in Zhu and Tsvankin (2006).

The attenuating VTI eikonal equation is complicated to solve analytically due to the existence of the fourth-order term. Therefore, we seek an approximate solution of the equation. Considering both η and A_z are relatively small in magnitude, we design a perturbation method to split the attenuating eikonal equation into a set of governing equations for the traveltime coefficients in the second-order perturbation solution. The benefit of this approach is that these governing equations have an analytical solution for a homogeneous medium. We apply the Shanks transform to the perturbation solution to improve its accuracy.

Parameterization 1

The first parameterization includes the parameters v_z, v_n and η as defined in Alkhalifah (2000) and the parameters A_z, ϵ_Q and δ_Q as defined in Zhu and Tsvankin (2006). The acoustic attenuating VTI eikonal equation under this parameterization is given as (Hao and Alkhalifah 2017b)

$$A_1\tau_{,x}^2 + B_1\tau_{,z}^2 + C_1\tau_{,x}^2\tau_{,z}^2 = 1, \tag{1}$$

with

$$A_1 = v_n^2\left(1+2\eta\right)\left[1 - 2ik_Q\left(1+\epsilon_Q\right)\right], \tag{2}$$

$$B_1 = v_z^2\left(1 - 2ik_Q\right), \tag{3}$$

$$\begin{aligned} C_1 = {} & \frac{v_z^2}{v_n^2}\left[\left(1-2ik_Q\right)v_n^2 - ik_Q\delta_Q v_z^2\right]^2 \\ & - v_z^2 v_n^2\left(1+2\eta\right)\left(1-2ik_Q\right)\left[1-2ik_Q\left(1+\epsilon_Q\right)\right], \end{aligned} \tag{4}$$

$$k_Q = \frac{A_z}{1-A_z^2}, \tag{5}$$

where the subscript '1' in A_1, B_1 and C_1 is used to indicate that these coefficients correspond to Parameterization 1, i is the imaginary unit, x and z correspond to the horizontal and vertical axes and τ denotes the complex-valued traveltime. $\tau_{,x}$ and $\tau_{,z}$ denote the first-order derivatives of τ with respect to x and z, respectively.

The second-order trial perturbation solution to equation (1) is defined as

$$\tau = \tau_0 + \sum_{i=1}^{2}\tau_i\ell_i + \sum_{i\le j=1}^{2}\tau_{ij}\ell_i\ell_j, \tag{6}$$

with

$$\ell_1 = ik_Q, \quad \ell_2 = \eta, \tag{7}$$

where τ_0, τ_i and τ_{ij} denote the zeroth-, first- and second-order traveltime coefficients, respectively. As we will see later, this formulation of the trial solution ensures that all of the traveltime coefficients and their governing equations are real valued.

Next, we plug the trial solution from equation (6) into equation (1) and expand the result with respect to ℓ_1 and ℓ_2 up to the second-order term. By comparing the coefficients for the zeroth-order term in the left- and right-hand sides of the resulting equation, we get the governing equation for τ_0:

$$v_n^2\tau_{0,x}^2 + v_z^2\tau_{0,z}^2 = 1. \tag{8}$$

Next, comparing the coefficients of the first-order terms in the left- and right-hand sides of that equation, we get the governing equation for τ_i $(i = 1, 2)$:

$$v_n^2\tau_{0,x}\tau_{i,x} + v_z^2\tau_{0,z}\tau_{i,z} = f_i(\tau_0). \tag{9}$$

Finally, we compare the coefficients for the second-order term to get the governing equation for τ_{ij} $(i \le j = 1, 2)$:

$$v_n^2\tau_{0,x}\tau_{ij,x} + v_z^2\tau_{0,z}\tau_{ij,z} = f_{ij}\left(\tau_0, \tau_1, \tau_2\right). \tag{10}$$

The complete expressions for f_i and f_{ij} are shown in Appendix A.

In the above system of equations (8)–(10), equation (8) governs the P-wave traveltimes in non-attenuating elliptically isotropic media. Once τ_0 is calculated from equation (8), τ_1 and τ_2 are computed using equation (9). Having computed τ_0, τ_1 and τ_2, we can then obtain the second-order traveltime coefficients τ_{11}, τ_{12} and τ_{22} by solving equation (10).

For a homogeneous medium, the solutions of equations (8) through (10) are given by

$$\tau_0 = \sqrt{\tau_x^2 + \tau_z^2}, \tag{11}$$

$$\tau_1 = v_n^{-2}\tau_0^{-3}\left\{\delta_Q v_z^2\tau_x^2\tau_z^2 + v_n^2\left[\left(1+\epsilon_Q\right)\tau_x^4 + 2\tau_x^2\tau_z^2 + \tau_z^4\right]\right\}, \tag{12}$$

$$\tau_2 = -\tau_0^{-3}\tau_x^4, \tag{13}$$

$$\begin{aligned} \tau_{11} = {} & -\frac{3}{2}v_n^{-4}\tau_0^{-7}\left\{v_z^4\delta_Q^2\tau_x^2\tau_z^2\left(\tau_x^4 - \tau_x^2\tau_z^2 + \tau_z^4\right)\right. \\ & + 2v_z^2v_n^2\delta_Q\tau_x^2\tau_z^2\left[\left(1-\epsilon_Q\right)\tau_x^4 + 2\left(1+\epsilon_Q\right)\tau_x^2\tau_z^2 + \tau_z^4\right] \\ & + v_n^4\left[\left(1+\epsilon_Q\right)^2\tau_x^8 + 4\left(1+\epsilon_Q+\epsilon_Q^2\right)\tau_x^6\tau_z^2\right. \\ & \left.\left. + 2\left(3+\epsilon_Q\right)\tau_x^4\tau_z^4 + 4\tau_x^2\tau_z^6 + \tau_z^8\right]\right\}, \end{aligned} \tag{14}$$

$$\begin{aligned} \tau_{12} = {} & -v_n^{-2}\tau_0^{-7}\tau_x^4\left\{3\delta_Q v_z^2\tau_z^2\left(\tau_x^2 - 2\tau_z^2\right)\right. \\ & \left. - v_n^2\left[\left(1+\epsilon_Q\right)\tau_x^4 + 2\left(1+4\epsilon_Q\right)\tau_x^2\tau_z^2 + \left(1-2\epsilon_Q\right)\tau_z^4\right]\right\}, \end{aligned} \tag{15}$$

$$\tau_{22} = \frac{3}{2}\tau_0^{-7}\tau_x^6\left(\tau_x^2 + 4\tau_z^2\right), \tag{16}$$

where

$$\tau_x = \frac{x}{v_n}, \quad \tau_z = \frac{z}{v_z}. \tag{17}$$

Having computed the above traveltime coefficients, we can accelerate the convergence of the perturbation-based expansion series by using the Shanks transform Bender and

Orszag (1978). We derive the following possible three traveltime solutions using the Shanks transform:

$$\tau^{(1)} = \tau_0 + \frac{(\tau_1\ell_1 + \tau_2\ell_2)^2}{\tau_1\ell_1 + \tau_2\ell_2 - \tau_{11}\ell_1^2 - \tau_{12}\ell_1\ell_2 - \tau_{22}\ell_2^2}, \tag{18}$$

$$\tau^{(2)} = \tau_0 + \tau_2\ell_2 + \tau_{22}\ell_2^2 + \frac{(\tau_1 + \tau_{12}\ell_2)^2\ell_1}{\tau_1 + \tau_{12}\ell_2 - \tau_{11}\ell_1}, \tag{19}$$

$$\tau^{(3)} = \tau_0 + \tau_1\ell_1 + \tau_{11}\ell_1^2 + \frac{(\tau_2 + \tau_{12}\ell_1)^2\ell_2}{\tau_2 + \tau_{12}\ell_1 - \tau_{22}\ell_2}. \tag{20}$$

In these three candidate solutions, $\tau^{(1)}$ is obtained by applying the Shanks transform with respect to both ℓ_1 and ℓ_2 parameters, while $\tau^{(2)}$ and $\tau^{(3)}$ are obtained by applying the Shanks transform with respect to ℓ_1 or ℓ_2, respectively. Later we will compare these candidate solutions and investigate which one results in better accuracy.

Parameterization 2

In Parameterization 2, we use the horizontal velocity v_x instead of the NMO velocity parameter v_n. The remaining parameters are common to both parameterizations. Substituting the relation between the NMO velocity and the horizontal velocity, namely $v_n = v_x/\sqrt{1+2\eta}$, the eikonal equation (1) can now be rewritten as

$$A_2\tau_{,x}^2 + B_2\tau_{,z}^2 + C_2\tau_{,x}^2\tau_{,z}^2 = 1, \tag{21}$$

where

$$A_2 = v_x^2\left[1 - 2\mathrm{i}k_Q\left(1+\epsilon_Q\right)\right], \tag{22}$$

$$B_2 = v_z^2\left(1 - 2\mathrm{i}k_Q\right), \tag{23}$$

$$\begin{aligned} C_2 = {} & \frac{v_z^2}{v_x^2\left(1+2\eta\right)}\left[\left(1 - 2\mathrm{i}k_Q\right)v_x^2 - \mathrm{i}k_Q\delta_Q v_z^2\left(1+2\eta\right)\right]^2 \\ & - v_z^2v_x^2\left(1 - 2\mathrm{i}k_Q\right)\left[1 - 2\mathrm{i}k_Q\left(1+\epsilon_Q\right)\right]. \end{aligned} \tag{24}$$

The subscript '2' in A_2, B_2 and C_2 is used to indicate that these coefficients correspond to Parameterization 2. The other parameters are as defined for equation (1).

The second-order trial solution for equation (21) is defined as

$$\tau = \tilde{\tau}_0 + \sum_{i=1}^{2}\tilde{\tau}_i\ell_i + \sum_{i\le j=1}^{2}\tilde{\tau}_{ij}\ell_i\ell_j, \tag{25}$$

where ℓ_1 and ℓ_2 are given in equation (7), $\tilde{\tau}_0$, $\tilde{\tau}_1$ and $\tilde{\tau}_{ij}$ denote the zeroth-, the first- and the second-order traveltime coefficients, respectively.

We substitute the trial solution from equation (25) into equation (21) and expand the resulting equation with respect to ℓ_1 and ℓ_2 up to the second-order term. By comparing the coefficients for the zeroth-order term between the left- and right-hand sides, we get the governing equation for $\tilde{\tau}_0$:

$$v_x^2\tilde{\tau}_{0,x}^2 + v_z^2\tilde{\tau}_{0,z}^2 = 1. \tag{26}$$

Next, we compare the coefficients of the first term to get the governing equation for $\tilde{\tau}_i$ $(i = 1, 2)$:

$$v_x^2\tilde{\tau}_{0,x}\tilde{\tau}_{i,x} + v_z^2\tilde{\tau}_{0,z}\tilde{\tau}_{i,z} = \tilde{f}_i(\tilde{\tau}_0). \tag{27}$$

Finally, by comparing the coefficients for the second-order term, we get the governing equation for $\tilde{\tau}_{ij}$ $(i \le j = 1, 2)$:

$$v_x^2\tilde{\tau}_{0,x}\tilde{\tau}_{ij,x} + v_z^2\tilde{\tau}_{0,z}\tilde{\tau}_{ij,z} = \tilde{f}_{ij}(\tilde{\tau}_0, \tilde{\tau}_1, \tilde{\tau}_2). \tag{28}$$

For brevity sake, we list the complete expressions for $\tilde{f}_i$ and $\tilde{f}_{ij}$ in Appendix B.

In the above system of equations (26)–(28), equation (26) governs the P-wave traveltimes in non-attenuating elliptically isotropic media. Once $\tilde{\tau}_0$ is calculated from equation (26), equations (27) and (28) are successively solved to obtain $\tilde{\tau}_i$ and $\tilde{\tau}_{ij}$.

For a homogeneous medium, the solutions of equations (26) through (28) are given by

$$\tilde{\tau}_0 = \sqrt{\tilde{\tau}_x^2 + \tilde{\tau}_z^2}, \tag{29}$$

$$\tilde{\tau}_1 = v_x^{-2}\tilde{\tau}_0^{-3}\left\{\delta_Q v_z^2\tilde{\tau}_x^2\tilde{\tau}_z^2 + v_x^2\left[\left(1+\epsilon_Q\right)\tilde{\tau}_x^4 + 2\tilde{\tau}_x^2\tilde{\tau}_z^2 + \tilde{\tau}_z^4\right]\right\}, \tag{30}$$

$$\tilde{\tau}_2 = \tilde{\tau}_0^{-3}\tilde{\tau}_x^2\tilde{\tau}_z^2, \tag{31}$$

$$\begin{aligned} \tilde{\tau}_{11} = {} & \frac{3}{2}v_x^{-4}\tilde{\tau}_0^{-7}\left\{\delta_Q^2 v_z^4\tilde{\tau}_x^2\tilde{\tau}_z^2\left(\tilde{\tau}_x^4 - \tilde{\tau}_x^2\tilde{\tau}_z^2 + \tilde{\tau}_z^4\right)\right. \\ & + 2v_z^2v_x^2\delta_Q\tilde{\tau}_x^2\tilde{\tau}_z^2\left[\left(1-\epsilon_Q\right)\tilde{\tau}_x^4 + 2\left(1+\epsilon_Q\right)\tilde{\tau}_x^2\tilde{\tau}_z^2 + \tilde{\tau}_z^4\right] \\ & + v_x^4\left[\left(1+\epsilon_Q\right)^2\tilde{\tau}_x^8 + 4(1+\epsilon_Q+\epsilon_Q^2)\tilde{\tau}_x^6\tilde{\tau}_z^2\right. \\ & \left.\left. + 2\left(3+\epsilon_Q\right)\tilde{\tau}_x^4\tilde{\tau}_z^4 + 4\tilde{\tau}_x^2\tilde{\tau}_z^6 + \tilde{\tau}_z^8\right]\right\}, \end{aligned} \tag{32}$$

$$\begin{aligned} \tilde{\tau}_{12} = {} & v_x^{-2}\tilde{\tau}_0^{-7}\tilde{\tau}_x^2\tilde{\tau}_z^2\left\{v_x^2\left[\left(1-3\epsilon_Q\right)\tilde{\tau}_x^4 + 2\left(1+3\epsilon_Q\right)\tilde{\tau}_x^2\tilde{\tau}_z^2 + \tilde{\tau}_z^4\right]\right. \\ & \left. + \delta_Q v_z^2\left[4\tilde{\tau}_x^4 - \tilde{\tau}_x^2\tilde{\tau}_z^2 + 4\tilde{\tau}_z^4\right]\right\}, \end{aligned} \tag{33}$$

$$\tilde{\tau}_{22} = -\frac{9}{2}\tilde{\tau}_0^{-7}\tilde{\tau}_x^4\tilde{\tau}_z^4, \tag{34}$$

with

$$\tilde{\tau}_x = \frac{x}{v_x}, \quad \tilde{\tau}_z = \frac{z}{v_z}. \tag{35}$$

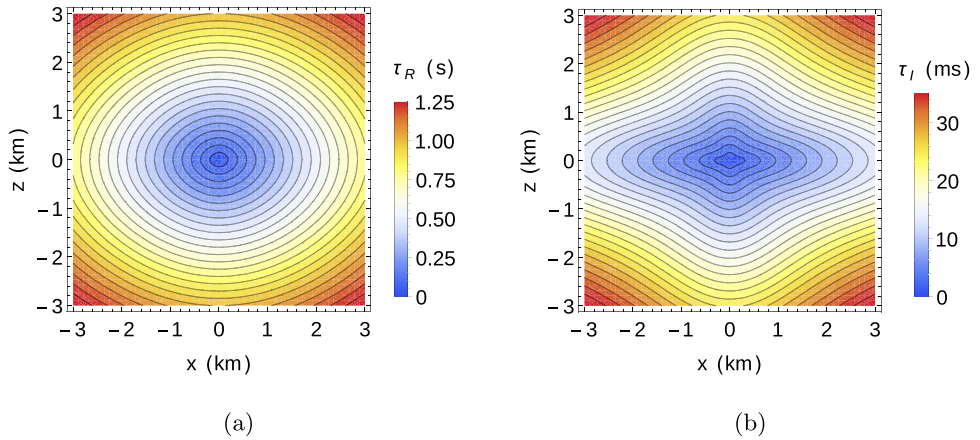

Figure 1 The exact traveltimes computed for a homogeneous attenuating VTI model. Plots (a) and (b) show the real and imaginary parts of the traveltimes, respectively. The model parameters are $v_z = 3.0$ km/s, $v_x = 3.795$ km/s, $\eta = 0.167$, $A_z = 0.02498$ (corresponding to $Q_{33} = 20$), $\epsilon_Q = -0.33$ and $\delta_Q = 0.98$. From these model parameters, the NMO velocity, $v_n = 3.286$ km/s.

We use the Shanks transform to derive three possible solutions for Parameterization 2, as follows:

$$\tilde{\tau}^{(1)} = \tilde{\tau}_0 + \frac{(\tilde{\tau}_1\ell_1 + \tilde{\tau}_2\ell_2)^2}{\tilde{\tau}_1\ell_1 + \tilde{\tau}_2\ell_2 - \tilde{\tau}_{11}\ell_1^2 - \tilde{\tau}_{12}\ell_1\ell_2 - \tilde{\tau}_{22}\ell_2^2}, \tag{36}$$

$$\tilde{\tau}^{(2)} = \tilde{\tau}_0 + \tilde{\tau}_2\ell_2 + \tilde{\tau}_{22}\ell_2^2 + \frac{(\tilde{\tau}_1 + \tilde{\tau}_{12}\ell_2)^2\ell_1}{\tilde{\tau}_1 + \tilde{\tau}_{12}\ell_2 - \tilde{\tau}_{11}\ell_1}, \tag{37}$$

$$\tilde{\tau}^{(3)} = \tilde{\tau}_0 + \tilde{\tau}_1\ell_1 + \tilde{\tau}_{11}\ell_1^2 + \frac{(\tilde{\tau}_2 + \tilde{\tau}_{12}\ell_1)^2\ell_2}{\tilde{\tau}_2 + \tilde{\tau}_{12}\ell_1 - \tilde{\tau}_{22}\ell_2}. \tag{38}$$

For equations (37) and (38), the Shanks transform is applied with respect to ℓ_1 and ℓ_2, respectively, while in equation (36), the Shanks transform is applied with respect to both ℓ_1 and ℓ_2.

NUMERICAL TESTS

In this section, we test the accuracy of the analytic solutions of the acoustic attenuating vertical symmetry axis (VTI) eikonal equation. We use the homogeneous VTI model with strong attenuation anisotropy as described by Hao and Alkhalifah (2017b).

For a comparison, we compute the exact traveltime by dividing the propagation distance by the complex ray velocity along the ray direction. The complex ray velocity vector is homogeneous for a homogeneous attenuating medium, meaning that the direction of the real part of the complex ray velocity vector is parallel to that of the imaginary part. For a given ray direction, we may invert for the slowness vector by numerically solving a system of non-linear equations with complex coefficients (Vavryčuk 2006). The complex ray velocity is directly calculated by substituting the obtained slowness vector into the ray tracing equations, allowing us to calculate the exact traveltime. The detailed procedure to calculate the complex ray velocity for an attenuating anisotropic medium can be found in Vavryčuk (2006, 2007).

Figure 1 shows the exact traveltimes in the homogeneous attenuating VTI model computed using the approach described above. It is noticeable that the imaginary part of the traveltimes shows stronger anisotropy signature than the real part of the traveltimes. These traveltime solutions will be compared against the solutions obtained for Parameterizations 1 and 2, and compared with the candidate solutions for the Shanks transform.

Figure 2 plots the absolute errors in the real part of the traveltimes computed using the expressions derived for Parameterization 1. We calculate the real part of the traveltimes using the second-order perturbation expression from equation (6) (Fig. 2a), using the Shanks transform expressions derived using (i) parameters ℓ_1 and ℓ_2 as given in equation (18) (Fig. 2b), (ii) parameter ℓ_1 as given by equation (19) (Fig. 2c) and (iii) parameter ℓ_2 as given by equation (20) (Fig. 2d) . We observe that the solution given by the Shanks transform expression in terms of parameter ℓ_2 yields the lowest absolute error (equation (20)).

In Fig. 3, we plot the absolute errors in the imaginary part of the traveltimes computed using the expressions derived for Parameterization 1. We calculate the imaginary part of the traveltimes in a similar way as described above. We observe that the Shanks transform expression derived using parameters ℓ_1 and ℓ_2 (equation (18)) is the most inaccurate. The other three solutions yield similar accuracy.

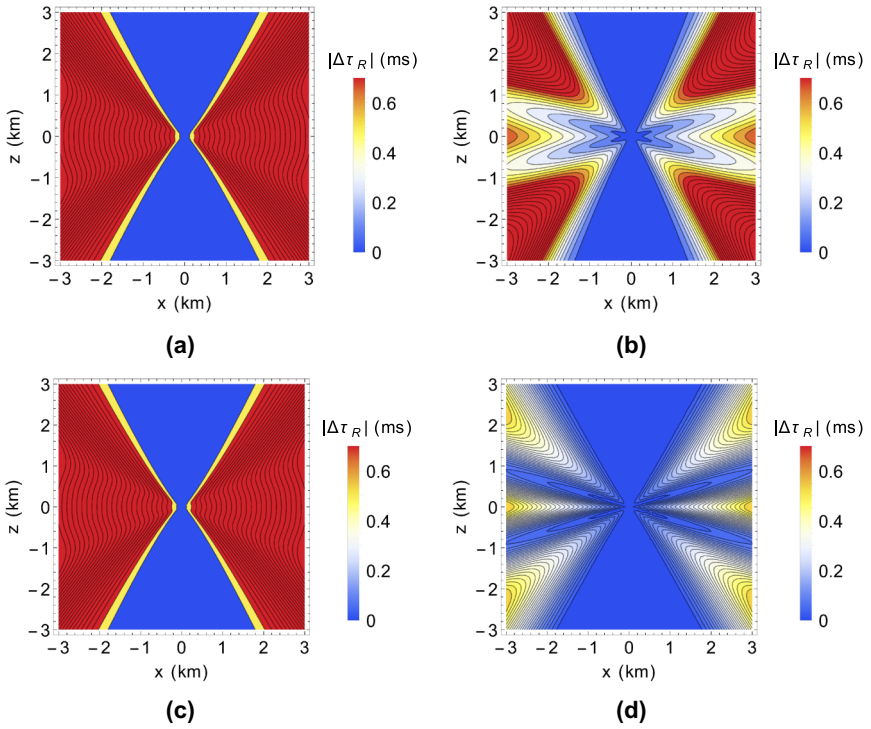

Figure 2 Absolute errors in the real part of the traveltimes from the analytic solutions corresponding to Parameterization 1 in the considered homogeneous attenuating VTI model. The plots correspond to (a) the solution using the second-order perturbation expression from equation (6), (b) the Shanks transform expression derived using parameters ℓ_1 and ℓ_2 as given by equation (18), (c) the Shanks transform expression derived using parameter ℓ_1 as given by equation (19) and (d) the Shanks transform expression derived using parameter ℓ_2 as given by equation (20). The model parameters are shown in the caption of Fig. 1.

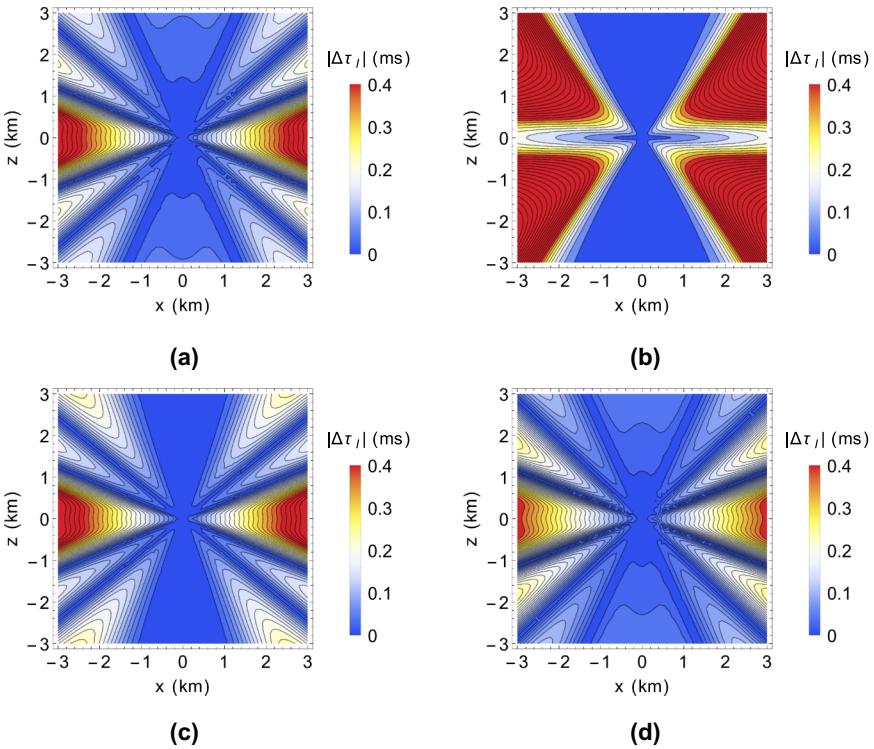

Figure 3 Absolute errors in the imaginary part of the traveltimes from the analytic solutions corresponding to Parameterization 1 in the considered homogeneous attenuating VTI model. The plots are corresponding to (a) the solution using the second-order perturbation expression from equation (6), (b) the Shanks transform expression derived using parameters ℓ_1 and ℓ_2 as given by equation (18), (c) the Shanks transform expression derived using parameter ℓ_1 as given by equation (19) and (d) the Shanks transform expression derived using parameter ℓ_2 as given by equation (20). The model parameters are shown in the caption of Fig. 1.

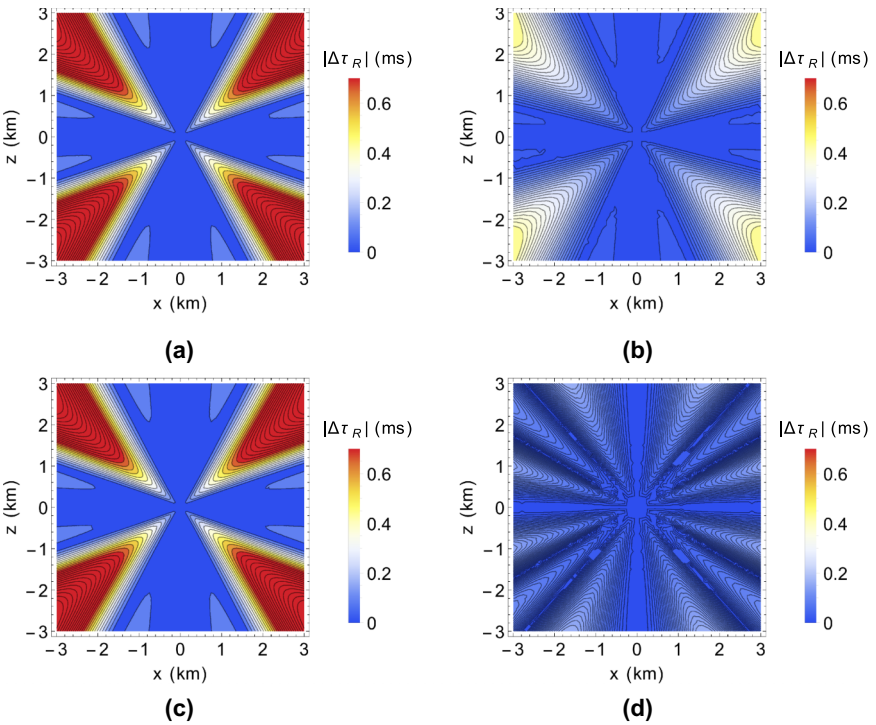

Figure 4 Absolute errors in the real part of the traveltimes from the analytic solutions corresponding to Parameterization 2 in the considered homogeneous attenuating VTI model. The plots are corresponding to (a) the solution using the second-order perturbation expression from equation (25), (b) the Shanks transform expression derived using parameters ℓ_1 and ℓ_2 as given by equation (36), (c) the Shanks transform expression derived using parameter ℓ_1 as given by equation (37) and (d) the Shanks transform expression derived using the parameter ℓ_2 as given by equation (38). The model parameters are shown in the caption of Fig. 1.

Similar to Fig. 2, in Fig. 4 we plot the absolute errors in the real part of the traveltimes, but this time computed using the expressions derived for Parameterization 2. By comparing the four candidate solutions, we observe that the Shanks transform expression derived using parameter ℓ_2 as given by equation (38) (Fig. 4d) yields the least absolute traveltime errors.

Likewise, Fig. 5 plots the absolute errors in the imaginary part of the traveltimes computed using the expressions derived for Parameterization 2. By comparing the four candidate solutions, we again observe that the Shanks transform expression derived using parameters ℓ_1 and ℓ_2 (equation (36)) is the most inaccurate. The other three solutions yield similar accuracy.

Figures 6 and 7 show an one-to-one accuracy comparison between the analytic solutions from these two parameterizations for a fixed radial distance. For the real part of the traveltimes at the propagation angles smaller than about 20°, all the analytic solutions from both parameterizations are accurate enough, although the analytic solutions from Parameterization 1 are slightly more accurate. For the real part of the traveltimes at the propagation angles between 40° and 60°, however, the analytic solutions from Parameterization 2 are typically more accurate than the corresponding ones from Parameterization 1. For the imaginary part of the traveltimes at the propagation angles less than 20°, all the analytic solutions are accurate and it is hard to identify which parameterization may lead to more accurate results. For the imaginary part of the traveltimes at the propagation angles between 20° and 50°, an overall comparison shows that Parameterization 1 leads to the more accurate analytic solutions than Parameterization 2. At the propagation angles larger than about 77°, any analytic solution from Parameterization 2 is much more accurate than the corresponding one from Parameterization 1 for both real and imaginary parts of the traveltimes. The maximum errors of the analytic solutions from Parameterization 2 are smaller than those from Parameterization 1.

An overall comparison of Figs 2–5 and Figs 6 and 7 shows that the Shanks transform expression derived using parameter ℓ_2 from Parameterization 2 (equation (38)) is the most accurate. As illustrated in plots (b) and (c) of Figs 2–5, the Shanks transforms with respect to both $\ell_1 = \mathrm{i}k_Q$ and $\ell_2 = \eta$ or only ℓ_1 are not helpful to improving the accuracy of the perturbation solutions.

To support the above analysis on a wide range of models, we design a number of attenuating VTI models (Table 1) by referring to Thomsen (1986), Zhu and Tsvankin (2006) and Shekar and Tsvankin (2011). Tables 2 and 3 compare the maximum relative errors in the real and imaginary parts of the traveltimes from the analytic solutions, respectively.

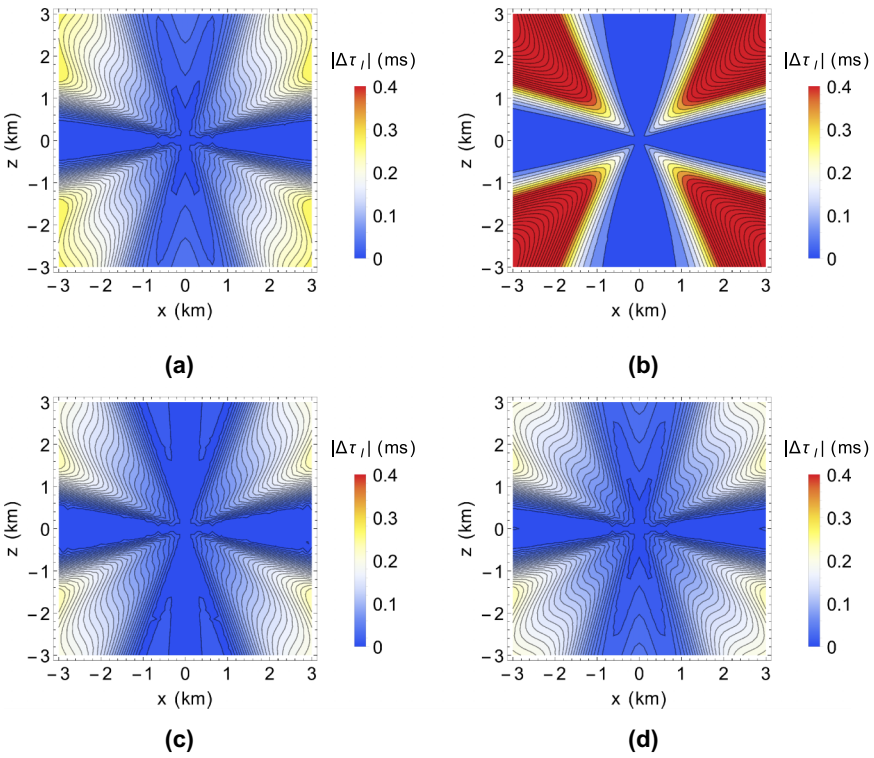

Figure 5 Absolute errors in the imaginary part of the traveltimes from the analytic solutions corresponding to Parameterization 2 in the considered homogeneous attenuating VTI model. The plots correspond to (a) the solution using the second-order perturbation expression from equation (25), (b) the Shanks transform expression derived using parameters ℓ_1 and ℓ_2 as given by equation (36), (c) the Shanks transform expression derived using parameter ℓ_1 as given by equation (37) and (d) the Shanks transform expression derived using parameter ℓ_2 as given by equation (38). The model parameters are shown in the caption of Fig. 1.

For the real part of the traveltimes, the Shanks transform expression derived using only parameter ℓ_2 from Parameterization 2 (equation (38)) is the most accurate among all the proposed analytic solutions. For the imaginary part of the traveltimes, the analytic solutions 25, 37 and 38 from Parameterization 2 are relatively accurate and have a comparable accuracy. As shown in Table 2, the Shanks transform expressions derived using both ℓ_1 and ℓ_2 (equations (18) and (36)) increase the approximation accuracy for the real part of the traveltimes by an order of magnitude compared with the second-order perturbation solutions (equations (6) and (25)). As illustrated in Table 3, in contrast, the same expressions (equations (18) and (36)) are much less accurate than the second-order perturbation solutions (equations (6) and (25)), respectively. For both real and imaginary parts of the traveltimes, the Shanks transform expressions derived using the parameter ℓ_1 from each parameterization (equation (19) or (37)) have almost the same approximation accuracy as the corresponding second-order perturbation expression (equation (6) or (25)). For each parameterization, the Shanks transform expression derived using the parameter ℓ_2 (equation (20) or (38)) has a higher accuracy than other analytic solutions.

An observation of the results in Tables 2 and 3 shows that Parameterization 2 results in a more accurate approximation for both the real and imaginary parts of the traveltimes than Parameterization 1. Overall, the Shanks transform expression derived using the parameter ℓ_2 from Parameterization 2 is the most accurate among all the analytic solutions.

In addition to the above analysis, we also find an interesting phenomenon: for the imaginary part of traveltimes, the Shanks transforms involving ℓ_1 as a perturbation parameter are unhelpful to improving the accuracy of the second-order perturbation expansions in most examples, especially for those formulated in Parameterization 1. ℓ_1 is the dominant parameter controlling the imaginary part of the traveltimes. For $\ell_1 = 0$, the acoustic attenuating eikonal equation becomes the non-attenuating one, and the imaginary part of the traveltimes vanishes. ℓ_2 does not have such an effect on both real and imaginary parts of the traveltimes. For an attenuating eikonal equation with $\ell_2 = 0$, the imaginary part of the traveltimes is still non-zero. Our numerical result illustrates that a dominant parameter like ℓ_1 cannot be used as a stable parameter to formulate the complex-valued version of a Shanks transform, although we are unable to prove this point mathematically.

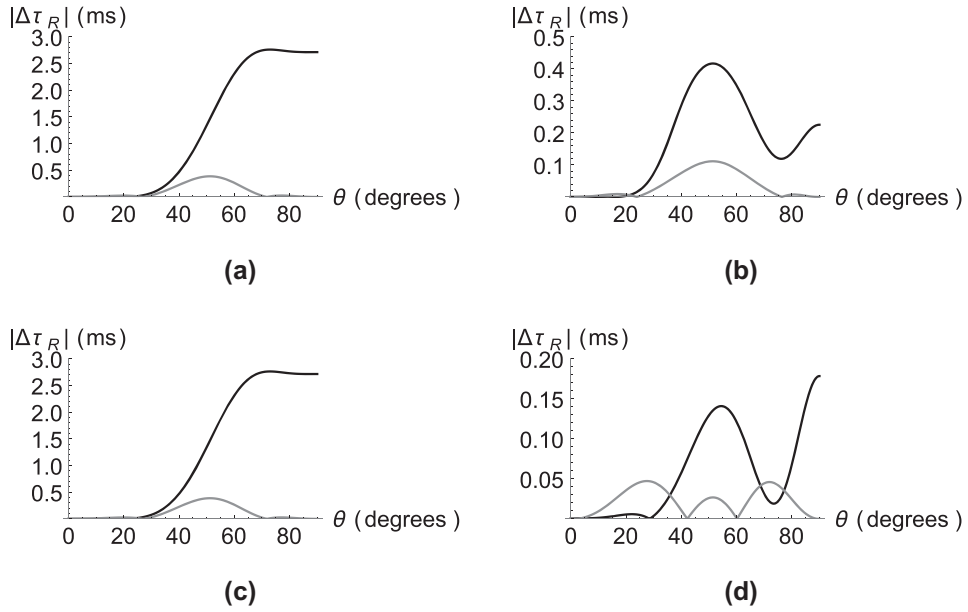

Figure 6 Absolute errors in the real part of the traveltimes at the propagation distance 1 km extracted from Figs 2 (black lines) and 4 (grey lines). The lateral coordinate θ denotes the propagation angle measured by a counterclockwise rotation from the vertically upward direction. Plots (a)–(d) correspond to the second-order perturbation expressions (equations (6) and (25)), the Shanks transform expressions derived using both parameters ℓ_1 and ℓ_2 (equations (18) and (36)), the Shanks transform expressions derived using parameter ℓ_1 (equations (19) and (37)), the Shanks transform expressions derived using parameter ℓ_2 (equations (20) and (38)), respectively.

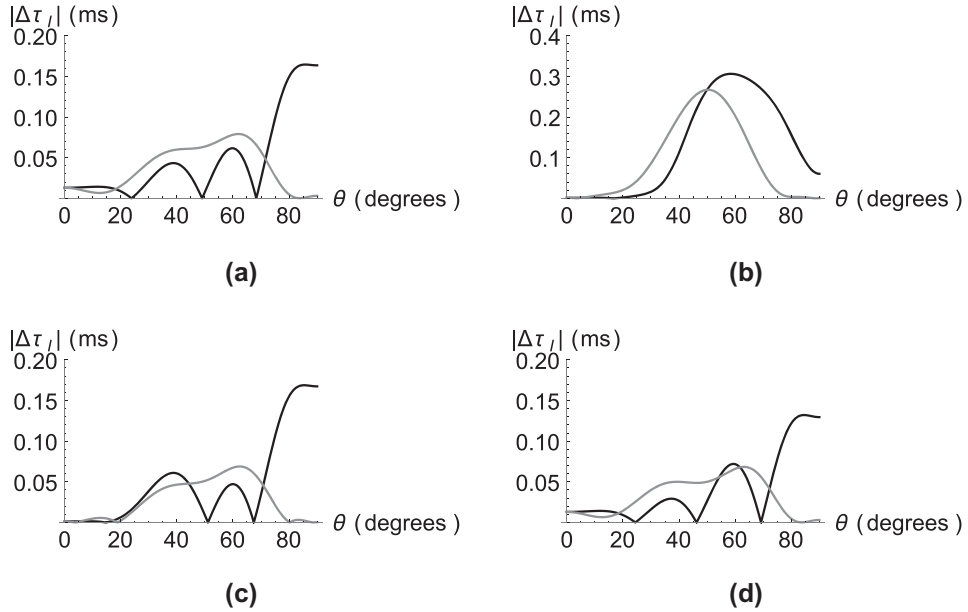

Figure 7 Absolute errors in the imaginary part of the traveltimes at the propagation distance 1 km extracted from Figs 3 (black lines) and 5 (grey lines). The lateral coordinate θ denotes the propagation angle measured by a counterclockwise rotation from the vertically upward direction. Plots (a)–(d) correspond to the second-order perturbation expressions (equations (6) and (25)), the Shanks transform expressions derived using both parameters ℓ_1 and ℓ_2 (equations (18) and (36)), parameter ℓ_1 (equations (19) and (37)) and parameter ℓ_2 (equations (20) and (38)), respectively.

Table 1 Medium parameters for the acoustic attenuating VTI models

Model	v_z (km/s)	v_n (km/s)	η	A_z/Q_{33}	ϵ_Q	δ_Q
Model 1	2.42	2.538	0.118	0.014/35	−0.3	−0.4
Model 2	1.862	2.082	0.125	0.005/100	0.2	0.1
Model 3	2.0	2.366	0.143	0.008/60	0.4	0.3
Model 4	1.6	1.824	0.115	0.0125/40	−0.3	0.2
Model 5	1.7	1.862	0.083	0.010/50	0.25	−0.15
Model 6	2.5	3.162	0.0625	0.008/60	0.4	0.3
Model 7	5.46	3.751	0.559	0.005/100	0.3	0.1
Model 8	3.962	3.592	0.175	0.010/50	0.3	0.64

The horizontal velocity in Parameterization 2 can be calculated by $v_x = v_n\sqrt{1+2\eta}$.

Table 2 Maximum relative errors in the real part of the traveltimes from the analytical solutions

	Parameterization 1				Parameterization 2			
Model	Taylor (%)	Shanks1 (%)	Shanks 2 (%)	Shanks 3 (%)	Taylor (%)	Shanks 1 (%)	Shanks 2 (%)	Shanks 3 (%)
Model 1	0.38	0.038	0.38	0.0267	0.052	0.009	0.052	0.0075
Model 2	0.44	0.035	0.44	0.033	0.06	0.009	0.06	0.0085
Model 3	0.66	0.054	0.66	0.046	0.09	0.015	0.09	0.0115
Model 4	0.35	0.033	0.35	0.026	0.048	0.009	0.048	0.0068
Model 5	0.135	0.016	0.135	0.0095	0.019	0.0046	0.019	0.0026
Model 6	0.056	0.0085	0.056	0.0038	0.008	0.0026	0.008	0.00095
Model 7	32.58	1.29	32.37	1.28	3.41	0.274	3.38	0.271
Model 8	1.20	0.092	1.19	0.081	0.156	0.026	0.156	0.018

All propagation directions are taken into account to determine the maximum relative errors for all models. In Parameterization 1, the terms 'Taylor', 'Shanks 1', 'Shanks 2' and 'Shanks 3' denote equations (6) and (18)–(20), respectively. In Parameterization 2, the similar terms denote equations (25) and (36)–(38), respectively.

DISCUSSION

We take into account Parameterizations 1 and 2 and utilize the perturbation theory and Shanks transform to derive the analytic traveltime solutions. The only difference between these two parameterizations is that Parameterization 1 involves the normal moveout (NMO) velocity but Parameterization 2 involves the horizontal velocity. Although we use the same perturbation parameters, Parameterizations 1 and 2 lead to different elliptically isotropic background media. The background medium corresponding to Parameterization 1 is described by the vertical velocity and the NMO velocity, while the one corresponding to Parameterization 2 is described by the vertical

Table 3 Maximum relative errors in the imaginary part of the traveltimes from the analytical solutions

	Parameterization 1				Parameterization 2			
Model	Taylor (%)	Shanks 1 (%)	Shanks 2 (%)	Shanks 3 (%)	Taylor (%)	Shanks 1 (%)	Shanks 2 (%)	Shanks 3 (%)
Model 1	1.91	3.14	1.91	1.62	0.42	1.21	0.39	0.41
Model 2	2.17	3.17	2.18	1.83	0.41	1.89	0.41	0.36
Model 3	2.87	3.67	2.90	2.28	0.60	2.47	0.57	0.51
Model 4	1.84	2.90	1.86	1.56	0.42	1.32	0.39	0.39
Model 5	1.05	1.44	1.08	0.90	0.22	0.75	0.19	0.21
Model 6	0.56	0.75	0.59	0.50	0.15	0.48	0.13	0.14
Model 7	35.79	23.68	35.82	18.87	5.68	19.42	5.70	2.92
Model 8	4.10	4.76	4.18	3.24	0.857	3.90	0.823	0.661

All propagation directions are taken into account to determine the maximum relative errors for all models. The terms 'Taylor', 'Shanks 1', 'Shanks 2' and 'Shanks 3' in Parameterizations 1 and 2 are explained in the caption of Table 2.

velocity and the horizontal velocity. Hence, the background medium corresponding to Parameterization 2 is closer to the non-attenuating vertical symmetry axis (VTI) medium than that corresponding to Parameterization 1, where the non-attenuating VTI medium is constructed by the real part of the stiffness coefficients of an attenuating VTI medium. As a result, the overall accuracy of any analytic solution from Parameterization 2 is higher than that of the corresponding analytic solution from Parameterization 1.

CONCLUSIONS

Parameterization 2 results in a more accurate approximation than Parameterization 1. For each parameterization, the Shanks transforms involving ik_Q as a parameter are not helpful to improving the accuracy of the second-order perturbation solution. The Shanks transform expression derived using only the anellipticity parameter from Parameterization 2 is the most accurate among all the proposed analytic solutions. It is noteworthy that the above conclusions are made from only a limited number of numerical experiments.

Although we only take into account the case of homogeneous attenuating vertical symmetry axis (VTI) media, the traveltime governing equations proposed in the paper can be used for an inhomogeneous attenuating VTI medium with constant η and A_z. We plan to design numerical techniques to solve the attenuating VTI eikonal equation for inhomogeneous media in the future.

ACKNOWLEDGEMENTS

The research was supported by the College of Petroleum Engineering and Geosciences at KFUPM. The authors are grateful for such support. Meanwhile, the authors thank Y. Ivanov and the anonymous reviewers for their reviews.

ORCID


Qi Hao https://orcid.org/0000-0003-3176-3222

REFERENCES

Alkhalifah T. 1998. Acoustic approximations for seismic processing in transversely isotropic media. *Geophysics* **63**, 623–631.

Alkhalifah T. 2000. An acoustic wave equation for anisotropic media. *Geophysics* **65**, 1239–1250.

Bender C.M. and Orszag S.A. 1978. *Advanced Mathematical Methods for Scientists and Engineers*. McGraw-Hill.

Červený V. and Pšenčík I. 2009. Perturbation hamiltonians in heterogeneous anisotropic weakly dissipative media. *Geophysical Journal International* **178**, 939–949.

Hao Q. and Alkhalifah T. 2017a. An acoustic eikonal equation for attenuating orthorhombic media. *Geophysics* **82**, WA67–WA81.

Hao Q. and Alkhalifah T. 2017b. An acoustic eikonal equation for attenuating transversely isotropic media with a vertical symmetry axis. *Geophysics* **82**, C9–C20.

Kravtsov Y.A., Forbes G.W. and Asatryan A.A. 1999. Theory and applications of complex rays. In: *Progress in Optics*, Vol. **39** (ed. E. wolf), pp. 1–62. Elsevier, Amsterdam.

Shekar B. and Tsvankin I. 2011. Estimation of shear-wave interval attenuation from mode-converted data. *Geophysics* **76**, D11–D19.

Thomsen L. 1986. Weak elastic anisotropy. *Geophysics* **51**, 1954–1996.

Tsvankin I. and Thomsen L. 1994. Nonhyperbolic reflection moveout in anisotropic media. *Geophysics* **59**, 1290–1304.

Vavryčuk V. 2006. Calculation of the slowness vector from the ray vector in anisotropic media. *Proceedings of the Royal Society. Series A, Mathematical and Physical Sciences* **462**, 883–893.

Vavryčuk V. 2007. Ray velocity and ray attenuation in homogeneous anisotropic viscoelastic media. *Geophysics* **72**, D119–D127.

Vavryčuk V. 2008. Real ray tracing in anisotropic viscoelastic media. *Geophysical Journal International* **175**, 617–626.

Vavryčuk V. 2012. On numerically solving the complex eikonal equation using real ray-tracing methods: a comparison with the exact analytical solution. *Geophysics* **77**, T109–T116.

Zhu Y. and Tsvankin I. 2006. Plane-wave propagation in attenuative transversely isotropic media. *Geophysics* **71**, T17–T30.

Zhubayev A., Houben M.E., Smeulders D.M. and Barnhoorn A. 2015. Ultrasonic velocity and attenuation anisotropy of shales, Whitby, United Kingdom. *Geophysics* **81**, D45–D56.

APPENDIX A: THE EXPRESSIONS FOR f_i AND f_{ij}

The expressions for f_i and f_{ij} in equations (9) and (10) are given by

$$f_1 = 1 + \delta_Q v_z^4 \tau_{0,x}^2 \tau_{0,z}^2 + \epsilon_Q (1 - v_z^2 \tau_{0,z}^2)^2, \tag{A1}$$

$$f_2 = -v_n^2 \tau_{0,x}^2 (1 - v_z^2 \tau_{0,z}^2), \tag{A2}$$

$$\begin{aligned} f_{11} = \frac{1}{2v_n^2} \{ & -v_n^4 \tau_{1,x}^2 + v_n^2 v_z^2 \tau_{1,z} (4\tau_{0,z} - \tau_{1,z}) \\ & + v_z^2 \tau_{0,x}^2 \tau_{0,z} [-\delta_Q v_z^2 (4v_n^2 (\tau_{0,z} - \tau_{1,z}) + \delta_Q v_z^2 \tau_{0,z}) \\ & + 4\epsilon_Q v_n^4 (\tau_{0,z} - \tau_{1,z})] \\ & + 4v_n^2 \tau_{0,x} \tau_{1,x} [\delta_Q v_z^4 \tau_{0,z}^2 + v_n^2 (1 + \epsilon_Q - \epsilon_Q v_z^2 \tau_{0,z}^2)] \}, \end{aligned} \tag{A3}$$

$$\begin{aligned} f_{12} = & -v_n^2 \tau_{1,x} \tau_{2,x} + v_z^2 \tau_{2,z} (2\tau_{0,z} - \tau_{1,z}) \\ & + 2\tau_{0,x}^2 \{ \delta_Q v_z^4 \tau_{0,z} \tau_{2,z} + v_n^2 [1 + \epsilon_Q - v_z^2 \tau_{0,z} (2\tau_{0,z} - \tau_{1,z} \end{aligned}$$

$$+\ \epsilon_Q(\tau_{0,z}+\tau_{2,z}))]\}$$
$$+\ 2\tau_{0,x}\left\{v_n^2\tau_{1,x}(-1+v_{P0}^2\tau_{0,z}^2)+\tau_{2,x}\left[\delta_Q v_{P0}^4\tau_{0,z}^2\right.\right.$$
$$\left.\left.+\ v_n^2(1+\epsilon_Q-\epsilon_Q v_{P0}^2\tau_{0,z}^2)\right]\right\}, \tag{A4}$$

$$f_{22}=\frac{1}{2}\left\{-v_n^2\tau_{2,x}(4\tau_{0,x}+\tau_{2,x})\right.$$
$$\left.+\ v_z^2\left[-\tau_{2,z}^2+4v_n^2\tau_{0,x}\tau_{0,z}(\tau_{0,z}\tau_{2,x}+\tau_{0,x}\tau_{2,z})\right]\right\}. \tag{A5}$$

APPENDIX B: THE EXPRESSIONS FOR $\tilde{f}_i$ AND $\tilde{f}_{ij}$

The expressions for $\tilde{f}_i$ and $\tilde{f}_{ij}$ in equations (27) and (28) are given by

$$\tilde{f}_1=1+\delta_Q v_z^4\tilde{\tau}_{0,x}^2\tilde{\tau}_{0,z}^2+\epsilon_Q(1-v_z^2\tilde{\tau}_{0,z}^2)^2, \tag{B1}$$

$$\tilde{f}_2=v_z^2v_x^2\tilde{\tau}_{0,x}^2\tilde{\tau}_{0,z}^2, \tag{B2}$$

$$\tilde{f}_{11}=\frac{1}{2v_x^2}\left\{-v_x^4\tilde{\tau}_{1,x}^2+v_z^2v_x^2\tilde{\tau}_{1,z}(4\tilde{\tau}_{0,z}-\tilde{\tau}_{1,z})\right.$$
$$+\ v_z^2\tilde{\tau}_{0,x}^2\tilde{\tau}_{0,z}\left[-\delta_Q v_z^2\left(4v_x^2(\tilde{\tau}_{0,z}-\tilde{\tau}_{1,z})+\delta_Q v_z^2\tilde{\tau}_{0,z}\right)\right.$$
$$\left.+\ 4\epsilon_Q v_x^4(\tilde{\tau}_{0,z}-\tilde{\tau}_{1,z})\right]$$
$$\left.+\ 4v_x^2\tilde{\tau}_{0,x}\tilde{\tau}_{1,x}\left[\delta_Q v_z^4\tilde{\tau}_{0,z}^2+v_x^2(1+\epsilon_Q-\epsilon_Q v_z^2\tilde{\tau}_{0,z}^2)\right]\right\}, \tag{B3}$$

$$\tilde{f}_{12}=-v_x^2\tilde{\tau}_{1,x}\tilde{\tau}_{2,x}+v_z^2\tilde{\tau}_{2,z}(2\tilde{\tau}_{0,z}-\tilde{\tau}_{1,z})$$
$$+\ 2v_z^2\tilde{\tau}_{0,x}^2\tilde{\tau}_{0,z}\left[\delta_Q v_z^2\tilde{\tau}_{2,z}+v_x^2(-2\tilde{\tau}_{0,z}+\tilde{\tau}_{1,z}-\epsilon_Q\tilde{\tau}_{2,z})\right]$$
$$+\ 2\tau_{0,x}\left\{v_z^2v_x^2\tilde{\tau}_{0,z}^2\tilde{\tau}_{1,x}+\tilde{\tau}_{2,x}\left[\delta_Q v_z^4\tilde{\tau}_{0,z}^2\right.\right.$$
$$\left.\left.+\ v_x^2(1+\epsilon_Q-\epsilon_Q v_z^2\tilde{\tau}_{0,z}^2)\right]\right\}, \tag{B4}$$

$$\tilde{f}_{22}=-\frac{1}{2}\left\{v_x^2\tilde{\tau}_{2,x}^2+v_z^2\left[\tilde{\tau}_{2,z}^2-4v_x^2\tilde{\tau}_{0,x}\tilde{\tau}_{0,z}\left(\tilde{\tau}_{0,z}\tilde{\tau}_{2,x}\right.\right.\right.$$
$$\left.\left.\left.+\ \tilde{\tau}_{0,x}(-\tilde{\tau}_{0,z}+\tilde{\tau}_{2,z})\right)\right]\right\}. \tag{B5}$$